Targeted Imaging of Colonic Tumors in Smad3$^{-/-}$ Mice Discriminates Cancer and Inflammation

Natasha G. Deane,[1,2,3] H. Charles Manning,[2,5] A. Coe Foutch,[1] M. Kay Washington,[7] Bruce A. Aronow,[8] Darryl J. Bornhop,[3,6] and Robert J. Coffey[3,4,9]

[1]Department of Surgery and Division of Surgical Oncology, [2]Department of Radiology and the Vanderbilt University Institute of Imaging Science, [3]Vanderbilt Ingram Cancer Center and [4]Departments of Medicine and Cell and Developmental Biology, Vanderbilt University, Nashville, Tennessee; Departments of [5]Neurosurgery, [6]Chemistry, [7]Pathology, and [8]Pediatrics at the Cincinnati Children's Hospital and the University of Cincinnati College of Medicine, Cincinnati, Ohio; and [9]Department of Medicine and the Department of Veterans Affairs Medical Center, Nashville, TN

Abstract

The peripheral benzodiazepine receptor (PBR) is a trans-mitochondrial membrane protein that modulates steroid biosynthesis. Recently, up-regulation and nuclear localization of PBR has been shown to be associated with colon, prostate, and breast cancer. PBR has been targeted by the exogenous synthetic ligand, PK11195, for various purposes including imaging. To capitalize on these observations, we developed a high-throughput, noninvasive, *in vivo* imaging approach to detect spontaneously arising colonic tumors in mice using a novel PBR-targeted molecular imaging agent (NIR-conPK11195). NIR-conPK11195 localized and was retained in colonic adenomas and carcinomas in Smad3$^{-/-}$ mice but not in non-neoplastic hamartomas or chronically inflamed colonic tissue. Using a fluorescence signal-to-noise ratio of ≥4-fold 13 h after injection of the agent, we detected colonic tumors with a sensitivity of 67% and a specificity of 86% in a cohort of 37 Smad3$^{-/-}$ mice and control littermates. Furthermore, using oral administration of dextran sulfate to induce colonic inflammation, we showed that the clearance profile of NIR-conPK11195 distinguished transient uptake in inflammatory tissue from longer term retention in tumors. Taken together, these results indicate that NIR-conPK11195 is a promising optical molecular imaging tool to rapidly screen for colonic tumors in mice and to discriminate inflammation from cancer.

(Mol Cancer Res 2007;5(4):341–9)

Introduction

Genetically engineered mouse models of human cancer represent a significant advance over conventional nude mouse xenograft models because it is possible to mimic features of human cancer development and progression by discrete spatial and temporal targeting of genetic events to distinct organs in the mouse. Adding to the relevance of these models, tumors from genetically engineered mouse models arise in immunocompetent hosts and are exposed to local factors of disease such as gut flora in the case of intestinal tumors. Among such models, Smad3$^{tm1par-/-}$ (hereafter referred to as Smad3$^{-/-}$ mice; ref. 1) have been shown to develop colonic tumors, including carcinomas, that exhibit a marked inflammatory component. In a recent advance, a single dose of azoxymethane has been coupled with the administration of dextran sulfate (DSS), which results in colonic inflammation (2) and then cancer. This combined approach produces cancers within the context of an inflammatory microenvironment, which has been shown to promote carcinogenesis in the gut (3, 4).

Preclinical assessment of tumor development and progression, as well as response to therapeutic intervention, in intestinal tumor models is currently limited by the lack of noninvasive methodologies suitable for evaluating the tumor. Thus, direct tumor assessment in these models requires sacrificing the animals, which complicates experimental protocols and significantly increases the number of animals required. Recently, others have reported advancement in the imaging of colonic tumors by contrast-enhanced computed tomography (CT) (5, 6) and by contrast-enhanced magnetic resonance imaging (MRI) (6). These techniques, while useful, remain low throughput and inherently invasive due to the necessity for purging, refilling, and suturing of the bowel to provide adequate contrast between the lumen of the bowel and the bowel wall. The development of accurate, low-cost, high-throughput, noninvasive imaging strategies capable of identifying tumor onset and progression, as well as response to treatment, remains an important goal toward rapid translation of innovative diagnostics and therapeutics.

The recent influx of low-cost instrumentation and novel molecular imaging reagents (7, 8) designed to operate within

Received 7/25/06; revised 12/21/06; accepted 1/31/07.
Grant support: NCI Mouse Models of Human Cancer Consortium (CA84239), NCI GI Special Program of Research Excellence (SPORE; CA95103), the Vanderbilt Ingram Cancer Center (CA68485) and the Vanderbilt Institute for Chemical Biology. H. C. Manning is supported by the Vanderbilt University Institute of Imaging Science, N. Deane is supported by NCI CA84239 and NIH DK52334. The Vanderbilt Microarray Shared Resource is supported by NIH CA68485 and by the Vanderbilt Diabetes Research and Training Center (DK20593), the Vanderbilt Digestive Disease Center (DK58404), the Genomics of Inflammation Program Project Grant (HL6744), and the Vanderbilt Vision Center (EY08126). The Mouse Metabolic and Phenotyping Core is supported by NCI DK59637. LI-COR Inc. is acknowledged for donating a portion of the dye employed.
The costs of publication of this article were defrayed in part by the payment of page charges. This article must therefore be hereby marked *advertisement* in accordance with 18 U.S.C. Section 1734 solely to indicate this fact.
Note: Supplementary data for this article are available at Molecular Cancer Research Online (http://mcr.aacrjournals.org/).
Requests for reprints: Darryl J. Bornhop, 5419 Stevenson VU Station B Box 351822, 1161 21st Avenue South, Nashville, TN 37235-1822. Phone: 615-322-4226. E-mail: Darryl.Bornhop@vanderbilt.edu

doi:10.1158/1541-7786.MCR-06-0225

the tissue-transparent near-IR (NIR) window has enabled rapid, systemic, deep tissue targeting of tumors in small animals. In this study, we developed a novel NIR imaging agent, NIR-conPK11195, to target the peripheral benzodiazepine receptor (PBR), which is up-regulated in late-stage colon cancer (9). PBR is primarily associated with mitochondrial steroidogenesis and has been shown to be up-regulated in the epithelial component of cancers of the colon, breast, and prostate (10), as well as in activated macrophages in the brain (11, 12). The PBR synthetic ligand, PK11195, has been used clinically to image inflammation associated with several neurologic diseases (13-15). Con-PK11195, an analogue of the widely used PBR ligand PK11195, was recently prepared (16) and shown to be useful as a targeting agent for fluorescent probes as well as bimodal lanthanide chelate-imaging agents (17).

Here, we prepared a NIR fluorophore-labeled version of the ligand, NIR-conPK11195, and tested it as a targeted imaging agent for colonic tumors in Smad3$^{-/-}$ mice. The accuracy of detecting colonic tumors was assessed by imaging a total of 37 mice [Smad3$^{-/-}$ (n = 25), Smad3$^{+/-}$ (n = 7), and Smad3$^{+/+}$ (n = 5) littermates]. Using fluorescence signal-to-noise ratio of ≥4-fold 13 h after injection of labeled ligand, the sensitivity and specificity of detecting adenomas and carcinomas were 67% and 86%, respectively. By this operationally defined criterion, small, flat lesions with invasive properties were detected but not benign tumors, chronically inflamed colon, or experimentally induced colonic inflammation. Overall, the imaging strategy we present provides a widely applicable, rapid, and inexpensive means of detecting colonic adenomas and carcinomas in the background of benign tumors and/or inflammation.

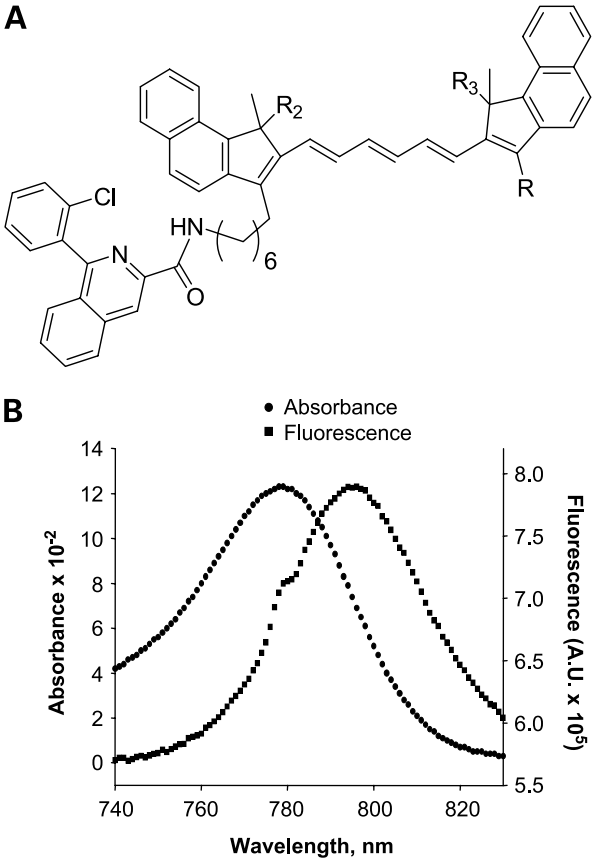

FIGURE 1. Structural and spectral characteristics of NIR-conPK11195. **A.** Chemical structure of NIR-conPK11195, an isoquinoline carboximide (*bottom left*), showing conjugation with LI-COR 800 W (*top right*) through a six-carbon linker. **B.** Spectral properties of NIR-con-PK11195 conjugate showing characteristic light absorbance (●) at 780 nm and emission (■) at 830 nm.

Results

Given the putative clinical relevance of PBR expression in human colon cancer (9), we queried PBR gene expression data from 39 colonic tumors derived from four distinct mouse models of intestinal neoplasia, including Smad3$^{-/-}$ (n = 13), azoxymethane-induced (n = 14), APC$^{Min+/-}$ (n = 9), and transforming growth factor β^{-};Rag2$^{-/-}$ tumors (n = 3). Expression values for 28,000 genes of known function were compared with those from wild-type (WT) adult C57BL6/J colons (n = 3). We found up-regulation of PBR expression in Smad3$^{-/-}$ tumors (mean log fold increase over adult WT colon = 3.6; SD, ±0.9), azoxymethane-induced tumors (mean log fold increase over adult WT colon = 3.0; SD, ±1.6), APC$^{Min/+}$ tumors (mean log fold increase over adult WT colon = 4.8; SD, ±3.3), and transforming growth factor β$^{-/-}$ × Rag2$^{-/-}$ tumors (mean log fold increase over adult WT colon = 4.3; SD, ±0.8; Supplementary Fig. S1A). Network analysis of gene expression changes clustering with respect to PBR up-regulation was conducted. This analysis indicated that PBR is coordinately regulated with genes that have emerged as master regulatory nodes in colon cancer such as p53, CEBP/β, and signal transducers and activators of transcription 3, and that it links to these nodes directly downstream of Myc (Supplementary Fig. S1B).

To develop an optical imaging agent capable of rapid and high-throughput imaging of deep-tissue PBR-expressing tumors, we labeled our novel analogue of the PBR ligand, con-PK11195 (16, 17), with a NIR fluorophore yielding the molecular imaging agent NIR-conPK11195 (Fig. 1A). The aqueous media spectroscopic properties of the resulting agent are shown in Fig. 1B, with excitation (λ_{max} = 780 nm) and emission (λ_{max} = 800 nm) centered within the tissue transparency window.

We next tested NIR-conPK11195 for specific retention in colonic tumors using 37 Smad3$^{-/-}$, Smad3$^{+/-}$, and Smad3$^{+/+}$ littermates between 2 and 5 months of age. For these experiments, we empirically selected a signal-to-noise ratio of ≥4-fold at 13 h after injection of labeled ligand as a cutoff for the prediction of the presence of tumor in the Smad3$^{-/-}$ mice. Using this operationally defined criterion, we evaluated NIR-conPK11195 signal retention in this cohort of mice. The results of this analysis are summarized in Table 1. Of the 37 animals tested, 15 harbored tumors, and 10 of these retained foci of NIR-conPK11195 fluorescent signal, thus producing 67% sensitivity (10/15) for tumor detection. Among the 22 non–tumor-bearing mice, only 3 retained foci of NIR-conPK11195 fluorescent signal 4-fold or higher above background, thus producing 86% specificity (19/22) for tumor detection.

To determine the kinetics of NIR-conPK11195 in live animals, we conducted clearance profile analyses upon the full

TABLE 1. Accuracy of NIR-conPK11195 Tumor Detection

	Pathologic result	
	Positive	Negative
Imaging result		
Positive	10	3
Negative	5	19
Total	15	22

NOTE: A signal-to-noise ratio ≥4-fold was used as the criterion for predicting tumors in a cohort of 37 mice [Smad$^{+/+}$ (n = 5), Smad3$^{+/-}$ (n = 7), Smad3$^{-/-}$ (n = 25)]. Imaging results were correlated with pathologic results upon sacrifice and analyzed using a contingency table as outlined in the table. Sensitivity, 10/15 (67%). Specificity, 19/22 (86%).

set of animals. For these experiments, 10 nmol of the agent was given i.v., and images were recorded before administration and at timed intervals up to 20 h postadministration (Fig. 2A). In Fig. 2B, we show a plot of the clearance profiles for age-matched Smad3$^{+/+}$ (left mouse) and Smad3$^{-/-}$ (right mouse) mice shown in Fig. 2A, using a uniform region of interest (ROI) to collect photon counts in the abdomen at locations avoiding the gall bladder where high focal background occurs (see ROI depicted in Fig. 2A). As can be seen, we observed little difference in focal fluorescent retention between control and Smad3$^{-/-}$ mice at early time points postadministration (<4 h) of NIR-conPK11195. However, between 4 and 7 h postadministration, the agent accumulated rapidly in the Smad3$^{-/-}$ mice and exhibited localized abdominal retention (≥4-fold over background per uniform ROI). Subsequently, the fluorescence intensity in both Smad3$^{-/-}$ and control animals gradually decreased, returning to background levels by 20 h postadministration. The presence or absence of colonic tumors in H&E-stained slides of intestinal "Swiss Rolls" was assessed by a pathologist (M.K. Washington), and PBR expression in the tumors was confirmed by immunohistochemistry. Here, strong nuclear staining of PBR can be seen in the epithelial component of intestinal tumors (Fig. 2D), consistent with published results (18). In contrast, there was weaker and more heterogeneous staining for PBR in normal colonic mucosa taken from control littermates (Fig. 2C).

To further examine the specificity of NIR-conPK11195 for tumors, the retention of free (unconjugated) NIR dye (LI-COR 800CW) was compared with the targeted chemistry (NIR-conPK11195) in Smad3$^{-/-}$ tumor-bearing animals. Images shown in Fig. 3 illustrate that free dye does not accumulate in the colons of tumor-bearing Smad3$^{-/-}$ mice following i.v.

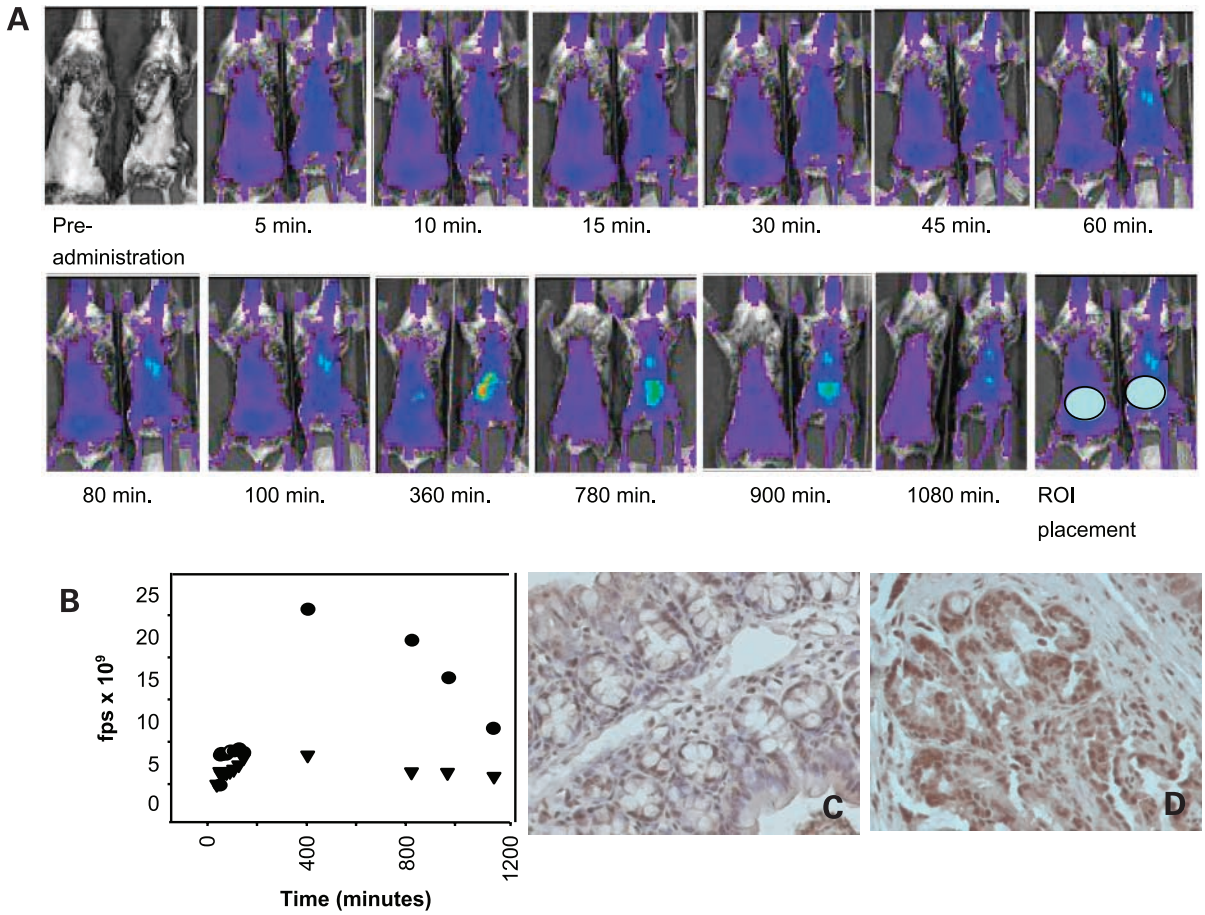

FIGURE 2. NIR-conPK11195 accumulates and is retained in colonic cancers of Smad3$^{-/-}$ mice. **A.** Smad3$^{+/+}$ (*left mouse in each picture*) and Smad3$^{-/-}$ (*right mouse in each picture*) mice were imaged and fluorescent signal quantified within a specified ROI (*last picture*) before and after administration of NIR-con-PK11195. **B.** Dynamic time-intensity curves for signal obtained from previous panels for tumor-bearing Smad3$^{-/-}$ (●) and their tumor-free Smad$^{+/+}$ (▼) siblings. **C.** PBR stain of normal colonic mucosa from Smad3$^{+/+}$ mouse imaged in A-M. **D.** Nuclear PBR staining in Smad3$^{-/-}$ tumor (magnification, 200×).

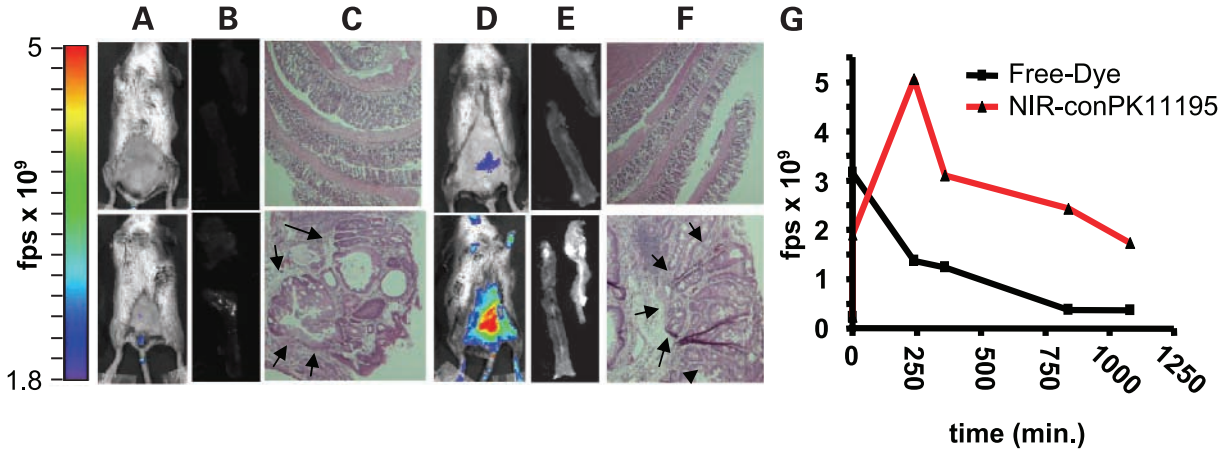

FIGURE 3. NIR-conPK11105 retention and colocalization with tumors is ligand dependent. Images of Smad3$^{+/+}$ (*top*) and Smad3$^{-/-}$ (*bottom*) mice injected with 10 nmol of unconjugated LI-Cor 800CW (**A,** *top* and *bottom*) or NIR-conPK11195 (**D,** *top* and *bottom*; signal intensity indicated by photon flux per second). **B** and **E.** High-resolution images (matched to **A** and **D**) of excised intestinal tissue show focal retention of NIR-conPK11195 in tumor-bearing mouse only (**E,** *bottom*). **C** and **F.** Matched H&E-stained slides at 50× magnification demonstrating normal mucosa from Smad3$^{+/+}$ mouse (*top*) and carcinoma from Smad3$^{-/-}$ mice (*bottom*). **G.** Clearance profiles of free dye versus NIR-conPK11195 in Smad3$^{-/-}$ tumor-bearing mice.

administration, nor does it produce signal at either low or high resolution (Fig. 3A and B, *bottom*). Furthermore, fluorescence of the free dye is comparable to control mice (Fig. 3A and B, *top*) signals. We also found that the free dye is rapidly cleared through the urinary tract and not through the hepatobiliary system, as is NIR-conPK11195 (data not shown). As seen in Fig. 3, high-resolution fluorescent imaging of excised colonic tissues following *in vivo* administration of the free dye or NIR-conPK11195 indicate ligand-specific focal retention in colonic cancer lesions intestinal at 13 h postadministration (Fig. 3B and E, *top* and *bottom*). Unconjugated LI-COR 800CW did not accumulate to a significant extent or colocalize with colonic tumors, nor did it accumulate in non–tumor-bearing animals (Fig. 3A-C, *top* and *bottom*). A clearance profile for representative tumor-bearing mice, shown in Fig. 3G, illustrates the relative photon flux per uniform ROI over time and shows ligand-specific retention of the agent. Therefore, accumulation and colocalization of NIR-conPK11195 is ligand dependent and is not due to nonspecific association with biological properties related to the tumor such as leaky vasculature.

To compare the optical imaging strategy with a more conventional imaging methodology, we imaged a set of Smad3$^{+/+}$ and Smad3$^{-/-}$ animals using ^{18}F-fluorodeoxyglucose (^{18}FDG)-positron emission tomography (PET) coregistered with CT and NIR-conPK11195. Representative images are shown in Fig. 4. We observed a good correlation between optical imaging using NIR-conPK11195 and PET imaging with ^{18}FDG for tumor detection in Smad3$^{-/-}$ mice. The presence of tumors could be detected using either imaging strategy at comparable resolution.

Upon close examination, we found variation in histopathology of tumors between Smad3$^{-/-}$ and Smad3$^{+/-}$ mice. This variation had apparent effects on the quantification of retained NIR-conPK11195 in these mice. Figure 5 shows a representative imaging experiment of Smad3$^{-/-}$ and Smad3$^{+/-}$ mice with accompanying histopathologic findings. As expected, we found adenomas and carcinomas in the Smad3$^{-/-}$ mice. In addition, benign lesions, such as hamartomas (Fig. 5B, *top*), and cystic lesions were identified only in Smad3 heterozygous mice. In live animal imaging, the NIR-conPK11195 fluorescent signature suggested varying degrees of labeling intensity among these mice. Representative examples show that benign hamartomas retained signal in the range of 1 to 2 × 10^8 photon flux per second (fps) (Fig. 5A, *top*), adenomas retained intermediate signal in the range of 2 to 3 × 10^8 fps (Fig. 5A, *middle*), and carcinomas retained signal above 3.5 × 10^8 fps (Fig. 5A, *bottom*). It is important to note that Smad3$^{-/-}$ animals with heavy tumor burden exhibited runting, resulting in a shorter path length for light to travel from the tumor through tissue, thus increasing the relative photon flux impinging onto the detector and complicating signal quantification between genotypes. Strategies to normalize signal to animal size should improve the quality of the information derived from deep tissue tumors and are currently under investigation.

In an effort to determine the effectiveness of detecting early lesions by NIR-conPK11195 imaging, we screened a panel of young Smad3$^{-/-}$ mice (aged 2 to 4 months). Because carcinomas in Smad3$^{-/-}$ mice are preceded by inflammation and dysplasia, these analyses allowed us to determine whether NIR-conPK11195 distinguished inflammation and dysplasia from cancer. As shown in Fig. 6A, NIR-conPK11195 was not retained in young Smad3$^{-/-}$ animals harboring significant inflammation, associated mucosal thickening, or dysplasia. One 4-month-old mouse in this group retained significant ≥4-fold (over background) NIR-conPK11195. Although initially overlooked by gross inspection, a single flat (sessile) adenocarcinoma was detected histologically in the excised tissue from this mouse (Fig. 6B, *right*, boundaries of tumor outlined by arrows). The invasive properties of this lesion were subsequently confirmed by our pathologist (M.K. Washington). This result suggests enhanced specificity of NIR-conPK11195 for invasive lesions, as suggested in Fig. 5 and will serve as the basis for further study on the role of PBR expression in tumor cell behavior.

Expression of PBR protein has been shown to be up-regulated in activated macrophages of the brain (11, 12). To determine whether NIR-conPK11195 would be retained by

intestinal inflammation, we administered NIR-conPK11195 to WT mice with colonic inflammation induced by a 7-day course of DSS in their drinking water according to the method of Cooper et al. (19). In these experiments, DSS-treated WT mice were imaged alongside untreated Smad3$^{-/-}$ mice. We found that significant NIR signal appeared abdominally at 4 and 8 h postadministration of NIR-conPK11195 in both tumor-bearing Smad3$^{-/-}$ and in DSS-treated WT animals. However, that fluorescent signal was retained at 13 h postadministration only in tumor-bearing animals (Fig. 7A). Strikingly, a rapid clearance of NIR signal occurred in the DSS-treated mice beginning between 4 and 8 h postadministration, as can be seen in the clearance profile (Fig. 7C). By 12 h postadministration, NIR signal returned to background levels in the DSS-treated mice, but not in the tumor-bearing Smad3$^{-/-}$ mice (Fig. 7A and B, *top* and *bottom*). Figure 7C depicts the mean fluorescence profile for DSS-treated and tumor-bearing mice between NIR-conPK11195 administration and 12 h thereafter. As can be seen in this profile, a 6-fold difference in signal was observed between Smad3$^{-/-}$ and DSS-treated WT mice. Upon tissue resection, we found patchy acute inflammation in sections from all DSS-treated animals accompanied by significant crypt degeneration, attenuated crypts, and significant loss of epithelium (Fig. 7B, *bottom*). Carcinomas were confirmed histologically for all Smad3$^{-/-}$ mice (Fig. 7B, *top*). Collectively, these data indicate that temporal behavior of NIR-conPK11195 retention can be used to discriminate neoplastic tissue from inflammation in Smad3$^{-/-}$ mice.

Discussion

We tested the effectiveness of a NIR-conPK11195–targeted imaging strategy in the Smad3$^{-/-}$ mouse model of intestinal cancer (for a review of the histopathology of these tumors as well as those from other experimental models of intestinal neoplasia, see ref. 20). Smad3$^{-/-}$ mice develop mucinous invasive carcinomas of the colon with a strong inflammatory component. We queried global tumor expression profiles from four mouse models of intestinal neoplasia for PBR expression. We found that PBR overexpression was uniformly up-regulated in mouse colonic tumors from all four mouse models. We did network analysis on a cluster of 11 genes that were coordinately regulated with PBR and found that 10 of these genes organized into a single network (Supplementary Fig. S1). This network analysis shows that PBR expression is regulated downstream of c-myc, and that its overexpression may serve as a broad marker for neoplasia and, thus, as a widely applicable imaging target. Therefore, we decided to use a NIR conjugate of the PBR ligand, PK11195, to test a targeted optical imaging strategy for colonic tumor detection in Smad3$^{-/-}$ mice. This strategy was sensitive and specific for colonic tumors and allowed us to rapidly screen a large cohort of mice for the presence of tumors on a background of colonic inflammation.

As illustrated in Fig. 2, we found by immunohistochemistry that overexpression of PBR in colonic tumors from Smad3$^{-/-}$ mice associates with nuclear accumulation of the protein. This is a novel finding for this protein in neoplastic colonic epithelium but is consistent with data from others (18, 21)

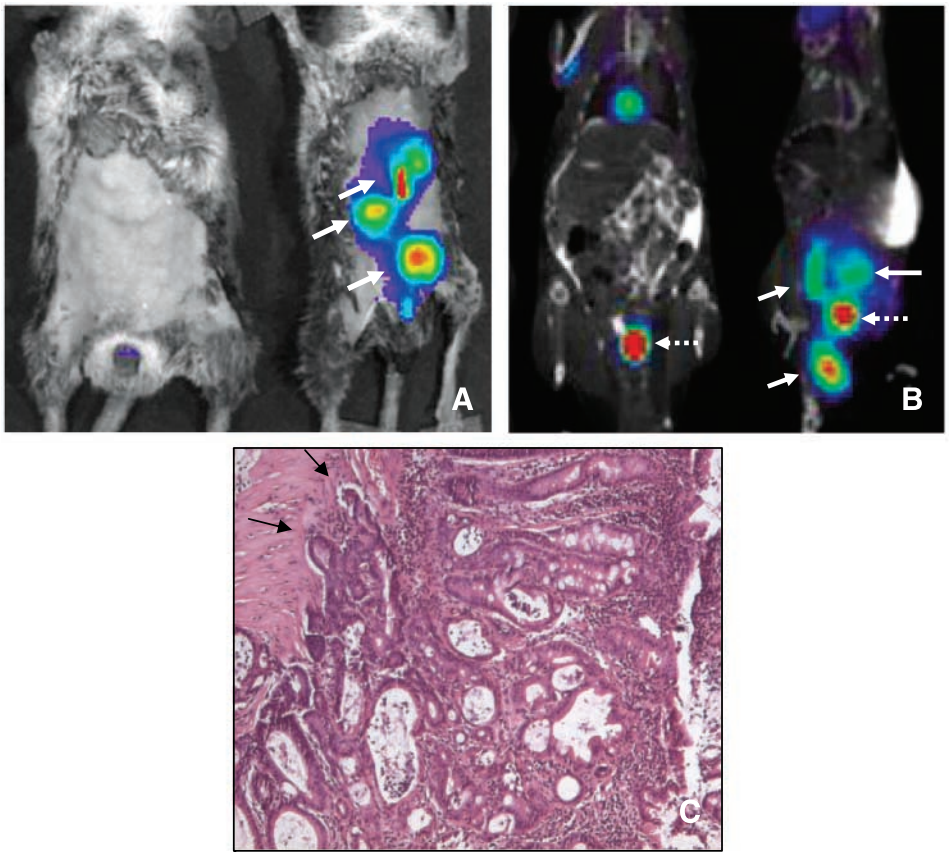

FIGURE 4. Compared resolution of NIR-conPK11195 imaging with ^{18}FDG-PET/CT imaging of colonic cancer in Smad3$^{-/-}$ mouse. Five-month-old WT (**A** and **B**, *left*) and Smad3$^{-/-}$ (**A** and **B**, *right*) mice were imaged sequentially. First, optically using NIR-conPK11195 (**A**) and then by ^{18}FDG-PET coregistered with contrast-enhanced CT (**B**). WT mice accumulate ^{18}FDG in the bladder (*dashed line*), whereas Smad3$^{-/-}$ mice have additional ^{18}FDG activity in areas corresponding to colonic tumors (*solid lines*) found at autopsy. H&E stain of colonic mucosa from animals imaged in (**A**) and (**B**) shown at 100× magnification. **C.** Smad3$^{-/-}$ mucosa demonstrating cancer characterized by laterally invasive epithelial cells (*arrows*).

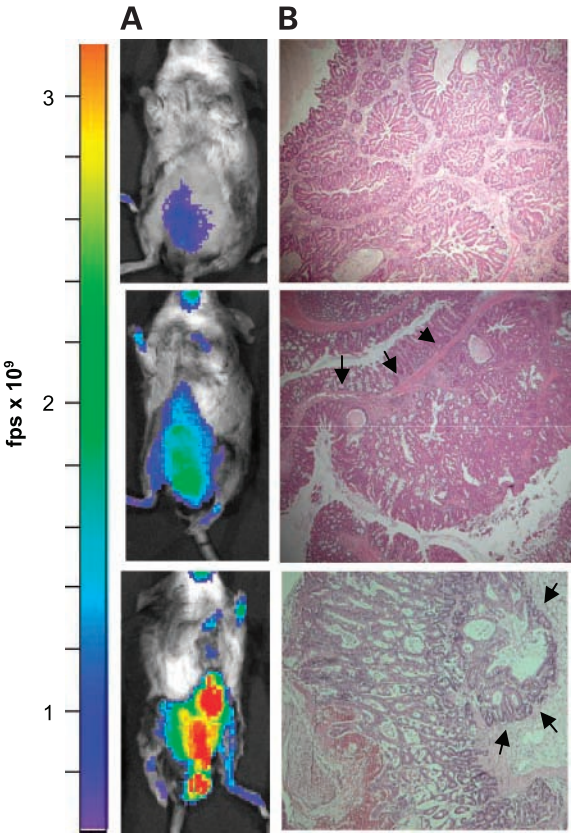

FIGURE 5. NIR-con-PK11195 is retained proportionately to tumor stage. **A.** Representative optical imaging of Smad3$^{+/-}$ (*top row*) and Smad3$^{-/-}$ (*middle and bottom row*) mice (fluorescence intensity indicated by photon flux per second). **B.** Matching H&E stains demonstrating hamartoma (*top row*; magnification, 100×), adenoma (*middle row*; magnification, 100×; *arrows,* uninterrupted muscularis mucosa), and carcinoma (*bottom row*; magnification, 50×; *arrows,* invasive component).

who have observed this phenomenon in both breast and in liver cancer cells. Although the role of nuclear PBR has not been precisely defined, it has been shown to exert an effect upon cellular proliferation in MDA-231 breast cancer cells (18).

Multiple methods for noninvasive assessment of intestinal tumors in mouse models have emerged over the past several years (5, 6, 22). The method presented here based on targeting PBR expression combines the low-cost, high-throughput advantages of optical methods based on bioluminescence, yet avoids the requirement for a reporter transgene enhancing the potential for translational usefulness. Although optical strategies have drawbacks in terms of spatial resolution and signal quantitation, we found these limitations to be comparable to those encountered with ^{18}FDG-PET/CT imaging (Fig. 4). Notably, however, the high-throughput nature of the optical screening strategy enabled high-throughput screening (up to 60 animals per hour is possible), whereas only a few animals could be screened by PET/CT imaging in a comparable time frame. Furthermore, screening the animals with optical imaging was accomplished at a fraction of the cost of PET/CT imaging, without the added complications of lengthy anesthesia or for the introduction of ionizing radiation. The advantage of this strategy lies in the fact that large populations of mice can be taken through an inexpensive and noninvasive screen, and more invasive and costly contrast-enhanced methods (PET, CT, or MRI) would be reserved for the subset of animals harboring tumors when appropriate. With respect to screening for the presence of colorectal cancer, the specificity (86%) and sensitivity (67%) reported here compares favorably with that obtained with comparable ^{18}FDG-PET data in humans reported at 91% to 93% sensitivity and 63% to 83% specificity (refs. 23, 24; considering the relative experience of trained radiologists versus laboratory scientists). No data exist to date regarding the detection specificity or sensitivity for intestinal lesion by ^{18}FDG-PET in mouse models.

The role of inflammation in cancer development is an area of intense investigation (2, 3). Previous studies have shown a high level of PBR expression in activated macrophages associated with inflammation (13, 25), so it was important for us to rule out nonspecific retention of the targeted agent related to tumor-associated inflammatory processes. We found that retention profiles of NIR-conPK11195 discriminated between mice treated with DSS and tumor-bearing mice at times between 8 and 13 h postadministration (Fig. 7C). Furthermore, we found that young mice exhibiting precancerous inflammation and associated epithelial dysplasia did not retain a NIR-conPK11195 (Fig. 6); however, in one animal from this group of younger animals, the presence of an invasive lesion correlated with significant NIR retention. Thus, NIR-conPK11195 represents an imaging agent that could be used to screen cohorts of mice during tumor development, even on the background of accompanying or experimentally induced inflammation.

The ability to follow molecular events *in vivo* represents a paradigm shift for medical science. A critically important goal of molecular imaging studies is to detect spontaneously arising tumors in the context of the host/tumor microenvironment (4). Smad3$^{-/-}$ mice exhibit many of the features of the tumor microenvironment of human colon cancer and, thus, represent an opportunity to study molecular features of disease progression and to assess therapeutic efficacy in preclinical trials. In a step toward these goals, we have shown an inexpensive, high-throughput strategy for *in vivo* molecular imaging of spontaneous intestinal neoplasia. Our ongoing efforts are directed toward preparing con-PK11195 analogues containing ^{99}Tc or ^{64}Cu to facilitate PBR targeting in clinically relevant imaging modalities, such as single-photon emission computed tomography (SPECT) and PET with the long-term goal of improving the early diagnosis of colon cancer. Additionally, we expect these agents to be useful for noninvasive monitoring of therapeutic efficacy that should be useful in improving clinical outcomes. These agents would be expected to achieve greater sensitivity and specificity than seen in this study when used in conjunction with detectors that have tomographic capability such as PET or SPECT.

Materials and Methods

Microarray

Data for PBR gene expression were obtained from a mouse colon tumor gene expression database composed of mouse tumors collected through the Mouse Models of Human Cancers Consortium.[10] Individual colonic tumors from individually

[10] http://emice.nci.nih.gov/

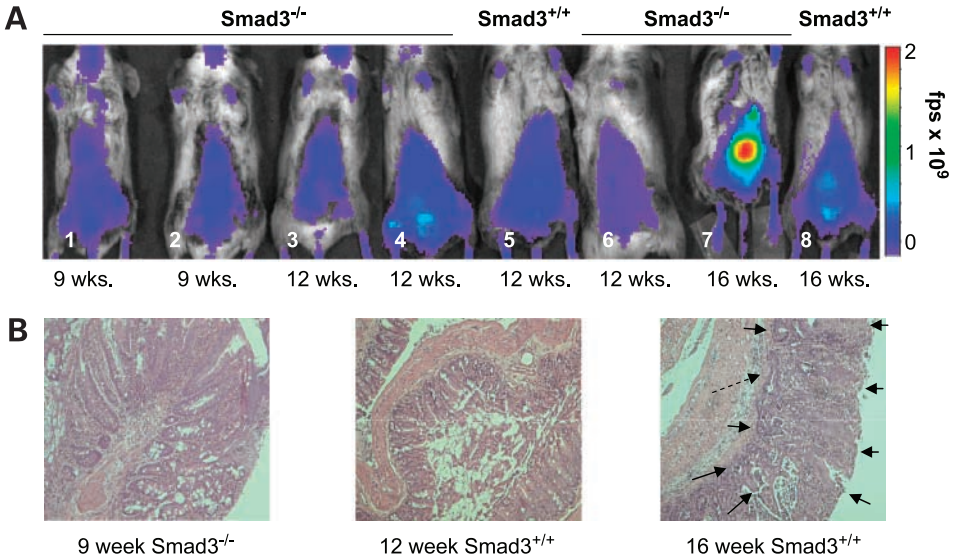

FIGURE 6. NIR-conPK11195 is not retained in dysplastic or inflammatory lesions of 2- to 3-month-old Smad3$^{-/-}$ mice. **A.** Smad3$^{-/-}$ mice (1-4, 6-7) and Smad3$^{+/+}$ control mice (5, 8), aged 9 to 16 wks as indicated, imaged optically using NIR-con-PK11195, show no focal accumulation of the imaging agent with the exception of mouse 7. **B.** Matching H&E-stained slides from select mice shown in (**A**), each at 100× magnification. Thickened colonic mucosa with inflammation and epithelial cell dysplasia taken from 9-week-old Smad3$^{-/-}$ mouse (*left*, taken from mouse 1 in **A**). Image of normal colonic mucosa (*middle*) was taken from mouse 5. Image of invasive flat lesion was taken from 16-week-old Smad3$^{-/-}$ mouse (7 in **A**). Solid arrows, outline of the lesion. Dashed arrow, tumor invasion into the muscularis mucosa.

excised tumors in various experimental strains were analyzed for PBR expression relative to normal C57BL6/J adult intestinal mucosa. The specific probe element for PBR was H3039E04 from a custom chip spotted at the Vanderbilt Microarray Core Facility representing 22,000 elements from the National Institute of Aging mouse cDNA library, 5,000 clones from Research Genetics, and 1,000 custom clones (28,000 cDNA elements total). Briefly, individual RNA samples were labeled with Cy5 as described by Park (26), and a universal reference RNA (day E17.5 whole mouse) was labeled with Cy3, hybridized to individual microarrays. Individual arrays were normalized by the Lowess intensity-dependent correction, and relative gene

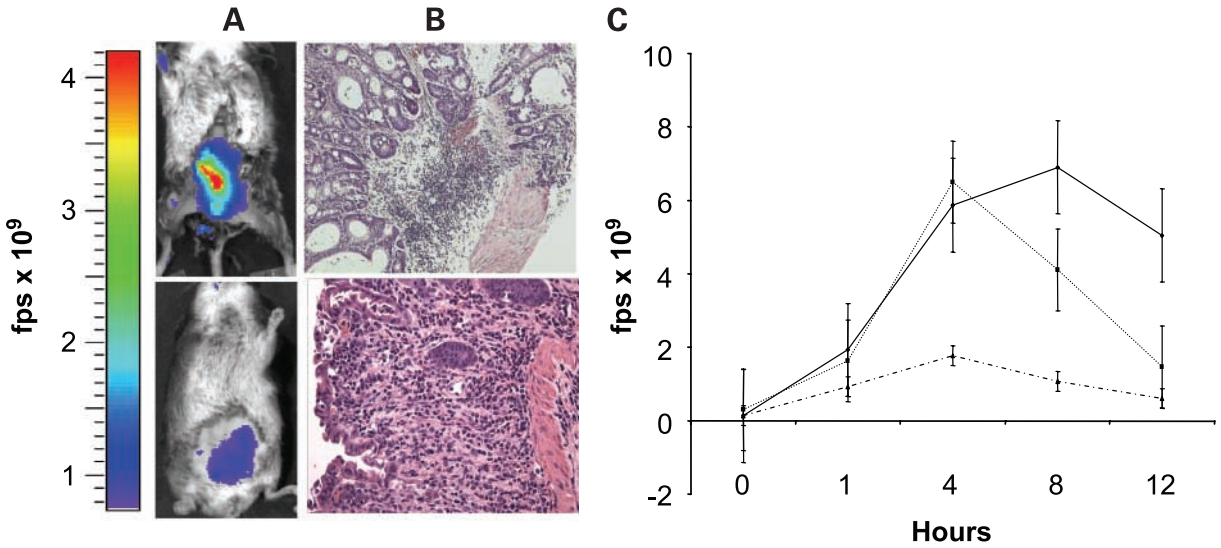

FIGURE 7. NIR-conPK11195 retention by inflammation is distinguishable from retention by tumor at late time points. **A.** Representative imaging of a 5-month-old Smad3$^{-/-}$ mouse (*top row*) and a 5-month-old WT mouse treated with DSS (*bottom row*). Optical images acquired at 13 h postadministration of NIR-conPK11195. **B.** Matched H&E-stained sections demonstrating invasive adenocarcinoma with inflammation in intestinal tissue taken from 5-month-old Smad3$^{-/-}$ mouse (*top*) and patchy crypt loss with a mixed acute and chronic inflammatory infiltrate in the lamina propria (magnification, 400×) in colonic tissue taken from WT DSS-treated mouse imaged in (*bottom*). Clearance curve for NIR-PK-11195 retention in tumor-bearing (*solid line*; $n = 7$), DSS-treated (*dotted line*; $n = 11$), and control (*dashed line*; $n = 4$) mice. Bars, SE at each time point.

expression levels were estimated by dividing individual gene signal ratios by that of the average of adult mouse colon samples. Gene network analysis was done using Ingenuity Pathway Analysis (Ingenuity Systems, Inc., Redwood City, CA).

Chemistry

Con-PK11195 was synthesized as described previously (16). LI-COR-800CW was purchased from LI-COR Biosciences (Lincoln, NE). Briefly, the dye and the conPK11195 derivative were dissolved by stirring in dry DMSO in an argon-flushed vessel. The reaction was protected from room light and allowed to proceed at room temperature overnight. Reaction progress was followed with reverse-phase HPLC using a C18 column and acetonitrile/water as the eluent. NIR-conPK11195 was purified on an open, alumina column eluting with acetonitrile/water, followed by an ion-exchange column eluting with water. Pure fractions were then concentrated using rotary evaporation and further concentrated with lyopholization. The imaging agent was characterized by nuclear magnetic resonance and electrospray ionization mass spectrometry calculated (found): 1364.01 (M^{2+} 681.95). Spectroscopic characterization in both water and DMSO consisted of both UV–visible light and fluorometry.

Mouse Models

Smad3$^{-/-}$ mice were maintained according to institutional guidelines. Induction of inflammation in mice was obtained according to the method of Cooper et al. (19). Briefly, adult mice were fed DSS (MW 40-50 kDa; U.S. Biochemical Co., Cleveland, OH) at 2.5% in the drinking water for 7 days at which time consumption of normal drinking water was resumed. Mice were imaged at days 9, 13, and 16 after commencement of the DSS treatment and sacrificed thereafter. Excised tissues were imaged on the Odyssey NIR imaging system (LI-COR Biosciences) using an 800-nm filter. Following *ex vivo* imaging, tissues were fixed in 4% paraformaldehyde for 8 to 12 h before dehydration in 70% ethanol and then paraffin embedded. H&E-stained slides were prepared, and pathology was ascertained by an experienced gastrointestinal pathologist (M.K. Washington).

Imaging Systems

Following i.v. administration of 10 nmol of NIR-conPK11195, *in vivo* imaging was carried out in a Xenogen IVIS 200 imaging system (Alameda, CA), equipped with a ventilator. Animals were anesthetized for imaging using 1.2% isoflurane (Baxter Pharmaceuticals, Deerfield, IL) in O_2 at 2 L/min. Body temperature was maintained using a thermostat-controlled heating pad. The Odyssey imaging system (see above) was used to image excised tissues using the 800-nm channel and 1-mm focus offset. Resolution and laser intensity were conserved during quantitative experiments.

For quantification of optical signal, uniform ROIs were created using the Xenogen software package. ROI area was conserved for each experiment, and the total photon flux was determined for individual ROIs. Signal-to-noise ratio was determined by dividing the ROI intensity for an experimental animal by the ROI intensity for the control animal.

For contrast-enhanced CT, 250 μL of 350 mg/mL organically bound iodine (Optiray 350, Mallinckrodt, Inc., St. Louis, MO) was injected i.p. immediately before imaging. Images were acquired with an 8-min exposure time at 80 kV with 360 projections over 360°, (125-μm isotropic voxel size). For micro-PET imaging, animals were injected i.p. with 120 to 180 μCi of ^{18}FDG. One hour later, the animal was anesthetized and positioned in the imaging cradle. For coregistration of CT and PET images, injections of iodinated triglyceride (Advanced Research Technologies Inc., Saint Laurent, Quebec, Canada) and FDG were timed such that imaging with the PET system immediately followed imaging with the CT system. A single imaging cradle, interchangeable with the CT and PET, was used such that mice could be imaged by both systems sequentially with minimal change in positioning. This imaging cradle had four fiducial markers that could be identified in both the PET and CT images. Image registration based on rigid-body alignment of these fiducials was achieved using the software package, Amide (27).

Histologic Analysis

Intestinal tissue was examined *in situ* for evidence of macroscopic tumors (>1 mm diameter). Sections of intestine were washed and prepared as a Swiss roll before preservation in 4% paraformaldehyde and subsequently paraffin embedded and sectioned for H&E staining. Five-micrometer tissue sections for immunohistochemistry were prepared as previously described (28). Primary rabbit anti-PBR polyclonal antibody (a generous gift from V. Papadopoulos, Georgetown University, Washington, DC) or anti-bromodeoxyuridine antibody (Accurate Chemical and Scientific Co., Westbury, NY) were used to stain sections using the Vectastin Elite ABC kit (Vector Laboratories, Burlingame, CA).

References

1. Zhu Y, Richardson JA, Parada LF, Graff JM. Smad3 mutant mice develop metastatic colorectal cancer. Cell 1998;94:703–14.

2. Okayasu I, Ohkusa K, Kajiura J, Kanno J, Sakamoto S. Promotion of colorectal neoplasia in experimental murine ulcerative colitis. Gut 1996;39:87–92.

3. Greten FR, Eckman L, Greten TF, et al. IKKβ links inflammation and tumorigenesis in a mouse model of colitis-associated cancer. Cell 2004;118:285–96.

4. Maggio-Price L, Treuting P, Zeng W, et al. *Helicobacter* infection is required for inflammation and colon cancer in SMAD3-deficient mice. Cancer Res 2006;66:828–38.

5. Pickhardt PJ, Halberg RB, Taylor AJ, et al. Microcomputed tomography colonography for polyp detection in an *in vivo* mouse tumor model. Proc Natl Acad Sci U S A 2005;102:3419–22.

6. Hensley HH, Chang WC, Clapper ML. Detection and volume determination of colonic tumors in Min mice by magnetic resonance micro-imaging. Magn Reson Med 2004;52:524–9.

7. Weissleder R, Ntziachristos V. Shedding light onto live molecular targets. Nat Med 2003;9:123–8.

8. Bremer C, Tung CH, Weissleder R. *In vivo* molecular target assessment of matrix metalloproteinase inhibition. Nat Med 2001;7:743–8.

9. Maaser K, Grabowski P, Sutter AP, et al. Overexpression of the peripheral benzodiazepine receptor is a relevant prognostic factor in stage III colorectal cancer. Clin Cancer Res 2002;8:3205–9.

10. Han Z, Slack RS, Li W, Papadopoulos V. Expression of peripheral benzodiazepine receptor (PBR) in human tumors: relationship to breast, colorectal, and prostate tumor progression. J Recept Signal Transduct Res 2003;23:225–38.

11. Banati RB. Visualising microglial activation *in vivo*. Glia 2002;40:206–17.

12. Cagnin A, Gerhard A, Banati RB. *In vivo* imaging of neuroinflammation. Eur Neuropsychopharmacol 2002;12:581–6.

13. Venneti S, Lopresti BJ, Wang G, et al. PET imaging of brain macrophages using the peripheral benzodiazepine receptor in a macaque model of neuroAIDS. J Clin Invest 2004;113:981–9.

14. Chen MK, Guilarte TR. Imaging the peripheral benzodiazepine receptor response in central nervous system demyelination and remyelination. Toxicol Sci 2006;91:532–9.

15. Gerhard A, Pavese N, Hotton G, et al. *In vivo* imaging of microglial activation with [11C](R)-PK11195 PET in idiopathic Parkinson's disease. Neurobiol Dis 2006;21:404–12.

16. Manning HC, Goebel T, Marx JN, Bornhop DJ. Facile, efficient conjugation of a trifunctional lanthanide chelate to a peripheral benzodiazepine receptor ligand. Org Lett 2002;4:1075–8.

17. Manning HC, Goebel T, Thompson RC, et al. Targeted molecular imaging agents for cellular-scale bimodal imaging. Bioconjug Chem 2004;15:1488–95.

18. Hardwick M, Fertikh D, Culty M, et al. Peripheral-type benzodiazepine receptor (PBR) in human breast cancer: correlation of breast cancer cell aggressive phenotype with PBR expression, nuclear localization, and PBR-mediated cell proliferation and nuclear transport of cholesterol. Cancer Res 1999;59:831–42.

19. Cooper HS, Murthy S, Kido K, Yoshitake H, Flanigan A. Dysplasia and cancer in the dextran sulfate sodium mouse colitis model. Relevance to colitis-associated neoplasia in the human: a study of histopathology, B-catenin and p53 expression and the role of inflammation. Carcinogenesis 2000;21:757–68.

20. Boivin GP, Washington K, Yang K, et al. Pathology of mouse models of intestinal cancer: consensus report and recommendations. Gastroenterology 2003; 124:762–77.

21. Corsi L, Geminiani E, Avallone R, Baraldi M. Nuclear location-dependent role of peripheral benzodiazepine receptor (PBR) in hepatic tumoral cell lines proliferation. Life Sci 2005;76:2523–33.

22. Sodir NM, Chen X, Park R, et al. Smad3 deficiency promotes tumorigenesis in the distal colon of ApcMin/+ mice. Cancer Res 2006;66:8430–8.

23. Arulampalam T, Costa D, Visvikis D, et al. The impact of FDG-PET on the management algorithm for recurrent colorectal cancer. Eur J Nucl Med 2001;28: 1758–65.

24. Kamel IR, Cohade C, Neyman E, Fishman EK, Wahl RL. Incremental value of CT in PET/CT of patients with colorectal carcinoma. Abdom Imaging 2004;29: 663–8.

25. Hardwick MJ, Chen MK, Baidoo K, Pomper MG, Guilarte TR. *In vivo* imaging of peripheral benzodiazepine receptors in mouse lungs: a biomarker of inflammation. Mol Imaging 2005;4:432–8.

26. Park YK, Franklin JL, Settle SH, et al. Gene expression profile analysis of mouse colon embryonic development. Genesis 2005;41:1–12.

27. Loening AM, Gambhir SS. AMIDE: a free software tool for multimodality medical image analysis. Mol Imaging 2003;2:131–7.

28. Deane NG, Parker MA, Aramandla R, et al. Hepatocellular carcinoma results from chronic cyclin D1 overexpression in transgenic mice. Cancer Res 2001;61: 5389–95.

Correction: Article on Optical Imaging of Intestinal Neoplasia

In the article on optical imaging of intestinal neoplasia in the April 2007 issue of *Molecular Cancer Research*, the name of an author, Bruce Aronow, was incorrect. His correct name is Bruce J. Aronow.

Deane NG, Manning HC, Foutch AC, et al. Targeted Imaging of Colonic Tumors in Smad3$^{-/-}$ Mice Discriminates Cancer and Inflammation. Mol Cancer Res 2007;5:341–9.

doi:10.1158/1541-7786.MCR-5-5-COR

Molecular Cancer Research

Targeted Imaging of Colonic Tumors in Smad3$^{-/-}$ Mice Discriminates Cancer and Inflammation

Natasha G. Deane, H. Charles Manning, A. Coe Foutch, et al.

Mol Cancer Res 2007;5:341-349.